Chapter 4
Comparative Study of SS316L Microstructural Response and Fracture Mechanisms under Isothermal vs. Adiabatic Dynamic Tensile Loading

Minoo Tayefeh Kazemi, Pooyan B. Javadzadeh, Bo Song, and Hongbing Lu

Abstract This study presents a direct comparison of the mechanical response and microstructural evolution of SS316L subjected to isothermal and adiabatic high-strain-rate tensile loading using a split Hopkinson tension bar system. Incremental loading was applied through controlled strain increments to allow thermal dissipation, whereas adiabatic loading was imposed in a single high-rate pulse. Electron backscatter diffraction (EBSD) analysis reveals progressive lattice distortion and grain subdivision in both loading modes. Prior to necking, deformation remains relatively homogeneous, although slightly higher local misorientation is observed under adiabatic loading. After necking, pronounced localization and crystallographic fragmentation developed in both cases, with more intense and spatially concentrated misorientation gradients in adiabatically loaded specimens. Fracture surfaces indicate ductile failure in both conditions, while adiabatic loading produces stronger shear-dominated features near the fracture. The results demonstrate that while the governing deformation mechanisms are comparable, thermal conditions significantly influence the severity and concentration of strain localization in the metastable austenitic stainless steel.

Keywords 316L stainless steel · split Hopkinson tension bar (SHTB) · high strain rate deformation · martensitic transformation · microstructural evolution

Introduction

Austenitic stainless steel 316L (SS316L) is widely used in structural and energy applications due to its high ductility, corrosion resistance, and weldability [1–7]. Its face-centered cubic (FCC) γ-austenitic structure, is stabilized by Ni, allowing plastic deformation through dislocation slip, deformation twinning (TWIP), and strain-induced martensitic transformation (TRIP), depending on strain and strain rate [8–10]. These mechanisms enhance strain hardening but also introduce microstructural heterogeneity at large strains.

Under high-strain-rate loading, such as that achieved with split Hopkinson tension bar techniques [9, 11], SS316L exhibits elevated flow stresses and strong competition between work hardening and thermal softening [12–14]. Near-adiabatic conditions can promote localized deformation and, in extreme cases, shear band formation [15–17]. While the dynamic deformation of 316L has been extensively studied, a direct comparison between adiabatic high-strain-rate tensile loading and controlled incremental tensile loading remains limited, particularly with respect to strain localization and lattice fragmentation.

The present work compares the mechanical response and microstructural evolution of SS316L subjected to adiabatic and incremental tensile loading. Using SEM and EBSD, emphasis is placed on quantifying strain localization and crystallographic fragmentation to clarify how deformation mode governs instability development in metastable austenitic steel.

Minoo Tayefeh Kazemi · Pooyan B. Javadzadeh · Hongbing Lu
Department of Mechanical Engineering, The University of Texas at Dallas, Richardson, TX 75080
e-mail: minoo.tayefehkazemi@utdallas.edu; pooyan.javadzadeh@utdallas.edu; hongbing.lu@utdallas.edu

Bo Song
Sandia National Laboratories, Albuquerque, NM, USA
e-mail: bsong@sandia.gov

© The Author(s), under exclusive license to River Publishers 2026

Kaitlynn Fitzgerald et al. (eds.), *Fracture, Fatigue, Failure and Thermomechanics & Infrared Imaging, Volume 4, 2026*,
Conference Proceedings of the Society for Experimental Mechanics Series, https://doi.org/10.13052/rp-9788743816270

Experimental Procedure

High-Strain-Rate and Incremental Tensile Testing

Dogbone-shaped SS316L tensile specimens were machined and threaded at both ends for attachment to a Kolsky tension bar system, following the procedure described by Song et al. [18]. Dynamic tensile tests were performed under two loading conditions: (i) adiabatic high-strain-rate loading using a single continuous pulse, and (ii) incremental isothermal loading using a modified Kolsky bar configuration [18].

In the incremental tests, specimens were loaded to predefined strain increments ($\sim$11%) at a controlled strain rate using a striker of predetermined length and velocity. Momentum-trapping devices prevented secondary loading pulses, ensuring single-pulse loading and elastic unloading after each increment. Engineering stress–strain curves were obtained from strain gauge signals mounted on the incident and transmission bars, while specimen displacement was monitored using a laser extensometer [19].

Microstructural Characterization

Following tensile testing, the specimens were sectioned longitudinally using a precision diamond cutter with oil cooling. Cross sections were mounted, mechanically polished to a mirror finish, and electropolished prior to microscopy.

Microstructural analysis was performed using a Zeiss Sigma 500 VP scanning electron microscope. Electron backscatter diffraction (EBSD) was conducted to characterize grain orientation, misorientation, and phase distribution. EBSD maps of samples prior to necking were collected from the uniform gauge section, while maps at the highest strain were obtained from the center of the necked region.

Secondary electron (SE) imaging was used to examine surface morphology and fracture features, including localized deformation zones and shear-related damage.

Results and Discussion

Mechanical Response

Engineering stress–strain curves obtained under adiabatic and incremental tensile loading reveal a clear strain-rate and thermal-condition dependence of plastic response. The adiabatic tests exhibit higher flow stress compared to incremental loading at comparable strain levels, consistent with positive strain-rate sensitivity reported for metastable austenitic steels [12–14].

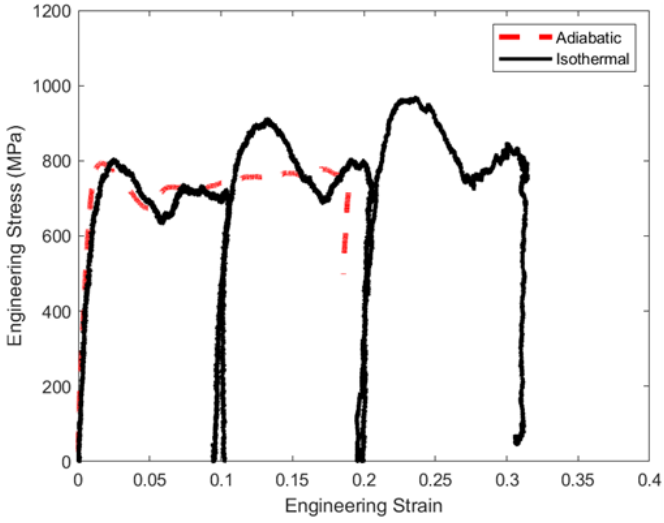

Fig. 1 Engineering stress vs. strain of adiabatic and isothermal specimens corresponding to 36% and 39% true strain respectively.

Under incremental loading, the stepwise deformation allows partial thermal dissipation between increments, leading to a more gradual hardening response. In contrast, the single-pulse adiabatic loading promotes rapid strain accumulation and limited heat transfer, while simultaneously accelerating instability development at large strains. The difference becomes more pronounced as the onset of localization approaches.

As shown in Figure 1 below, the engineering stress–strain comparison is only valid up to the onset of necking. Beyond this point, engineering measurements no longer represent the intrinsic material response because deformation becomes highly localized within the specimen. Therefore, we calculated the true strain based on post-test diameter of the specimens:

$$\varepsilon_{true} = \ln\frac{A_0}{A_f} = 2\ln\frac{D_0}{D_f} \tag{1}$$

where A_0 and A_f are the initial and final cross-sectional areas of the specimen, respectively, and D_0 and D_f are the corresponding initial and final diameters of the specimen, respectively. In this study we used true strain for comparison of isothermal and adiabatically elongated specimens.

Microstructural Evolution Prior to Necking

Figure 2 below shows inverse pole figure (IPF) and kernel average misorientation (KAM) during EBSD analysis of both adiabatic and isothermal specimens at 36% and 39% strain, respectively. EBSD analysis of specimens prior to necking indicates progressive lattice distortion and grain subdivision in both loading modes. IPF maps show increasing orientation heterogeneity within grains, while KAM maps reveal elevated local misorientation values corresponding to dislocation accumulation and plastic strain. Although both conditions activate similar deformation mechanisms at these strain levels, the adiabatic specimens display higher local misorientation concentrations, suggesting more intense dislocation storage under rapid loading. However, deformation remains relatively homogeneous prior to necking.

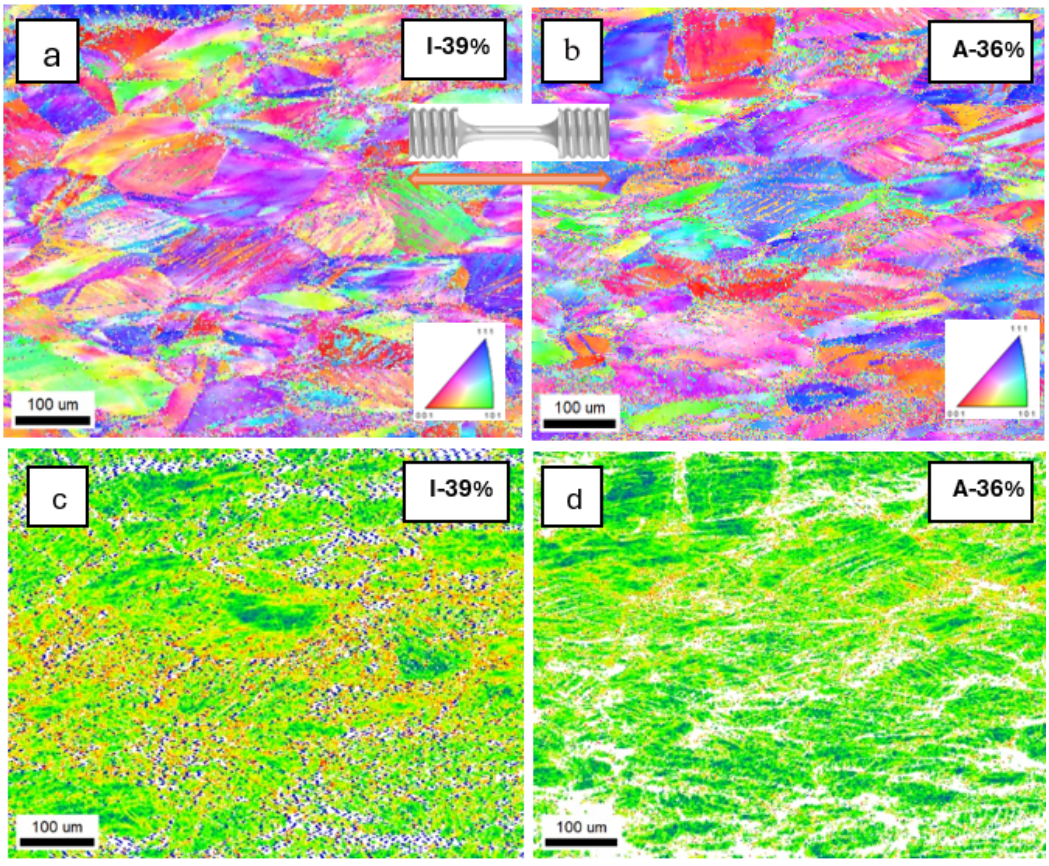

Fig. 2 EBSD inverse pole figure (IPF) and kernel average misorientation (KAM) maps of SS316L specimens deformed under dynamic tension at: (a & c) Isothermally 39%, and (b & d) adiabatically 36%

Strain Localization and Fragmentation post-necking

At higher strain levels, deformation becomes strongly localized. EBSD maps reveal pronounced grain fragmentation and elevated lattice curvature in both loading modes. The KAM distributions demonstrate concentrated high-misorientation regions associated with strain localization.

Figure 3 below shows that the severity of fragmentation is greater in the adiabatic condition, where localized misorientation gradients are more intense and spatially concentrated. This behavior is attributed to the combined effects of strain-rate sensitivity and near-adiabatic heating, which intensify instability development by amplifying the competition between strain hardening and thermal softening [12–15].

Despite these differences in severity, both loading modes produce comparable qualitative deformation features, including grain subdivision and high dislocation density, indicating that the fundamental deformation mechanisms remain similar while the degree of localization is strongly influenced by the loading condition.

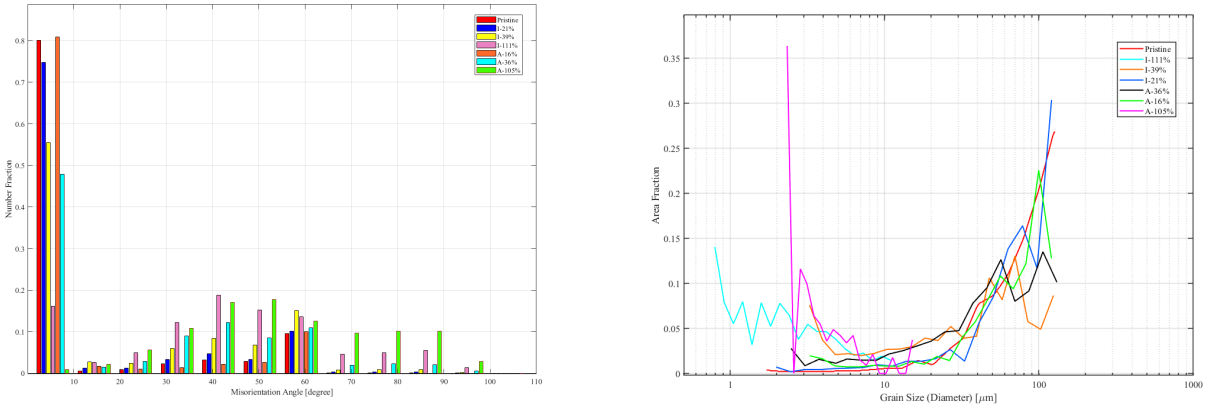

Fig. 3 Misorientation angle distributions and grain size distributions of SS316L specimens subjected to dynamic tensile loading at various strain levels.

Fracture Characteristics

Secondary electron imaging of fracture surfaces in Figure 4 shows ductile failure in both cases, characterized by microvoid coalescence. However, the adiabatic specimens exhibit more pronounced shear-dominated features and localized deformation zones near the fracture. This observation is consistent with the intensified strain localization identified in EBSD analysis and aligns with prior reports of dynamic localization in SS316L under rapid loading [11, 15].

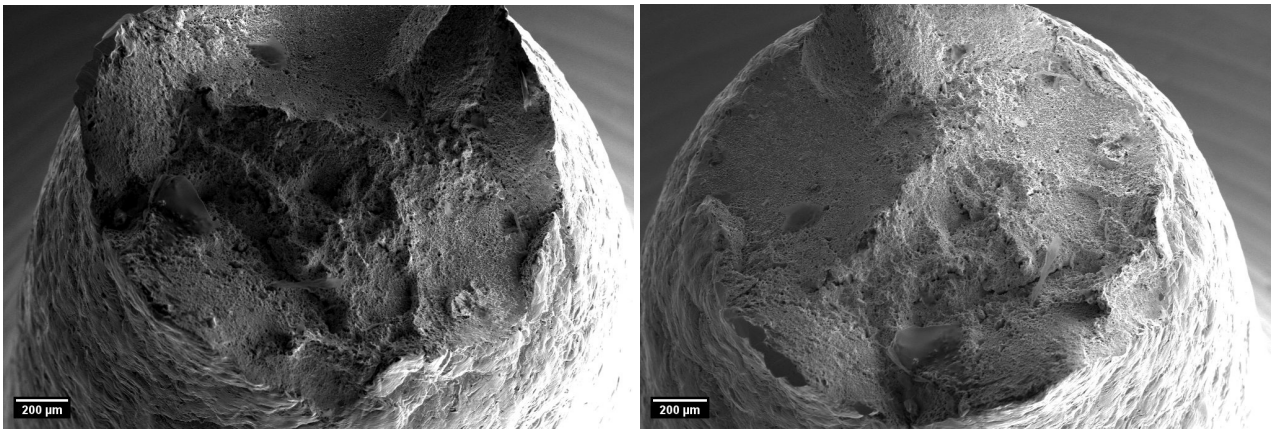

Fig. 4 SEM images of fracture surfaces of stainless-steel specimens tested isothermally (right) and adiabatically (left).

Conclusion and Future Work

SS316L subjected to adiabatic and incremental tensile loading exhibits similar deformation mechanisms but different levels of localization. Adiabatic loading produces higher flow stress and more intense, spatially concentrated lattice misorientation compared to incremental loading. EBSD confirms progressive grain fragmentation in both conditions, with stronger strain localization under near-adiabatic deformation. Fracture remains ductile in both cases, though shear-dominated features are more pronounced in dynamically loaded specimens.

Future work will focus on quantitative misorientation analysis and interrupted testing to characterize localization evolution prior to and during necking, as well as phase-sensitive characterization to assess strain-induced transformation under dynamic loading.

Acknowledgments We acknowledge the support of the Department of Energy, National Nuclear Security Administration, Predictive Science Academic Alliance Program (PSAAP) under Award Number DE-NA0003962. We also thank the support of NSF under 2219347 & 1726435, and DoE under DoE DE-NA0003962 and DE-NA-0003525. Lu also acknowledges the Louis A. Beecherl Jr. chair for additional support.

This work was performed under the Laboratory Directed Research and Development (LDRD) program at Sandia National Laboratories. Sandia National Laboratories is a multi-mission laboratory managed and operated by National Technology & Engineering Solutions of Sandia, LLC (NTESS), a wholly owned subsidiary of Honeywell International Inc., for the U.S. Department of Energy's National Nuclear Security Administration (DOE/NNSA) under contract DE-NA0003525. This written work is authored by an employee of NTESS. The employee, not NTESS, owns the right, title and interest in and to the written work and is responsible for its contents. Any subjective views or opinions that might be expressed in the written work do not necessarily represent the views of the U.S. Government. Authors would like to thank Dr. Angela Ku for providing the samples.

References

1. M.J. Sohrabi, M. Naghizadeh, H. Mirzadeh, Deformation-induced martensite in austenitic stainless steels: A review, Arch. Civ. Mech. Eng. 20 (2020) 124. https://doi.org/10.1007/s43452-020-00130-1.
2. K. Nalepka, B. Skoczeń, M. Ciepielowska, R. Schmidt, J. Tabin, E. Schmidt, W. Zwolińska-Faryj, R. Chulist, Phase Transformation in 316L Austenitic Steel Induced by Fracture at Cryogenic Temperatures: Experiment and Modelling, Materials 14 (2020) 127. https://doi.org/10.3390/ma14010127.
3. D. Bhoyar, N. Mungle, A review of microstructure, mechanical properties, and welding of SS316L, in: Recent Adv. Mater. Manuf. Mach. Learn., 1st ed., CRC Press, London, 2024: pp. 639–648. https://doi.org/10.1201/9781003450252-77.
4. R. Song, J. Xiang, D. Hou, Characteristics of Mechanical Properties and Microstructure for 316L Austenitic Stainless Steel, J. Iron Steel Res. Int. 18 (2011) 53–59. https://doi.org/10.1016/S1006-706X(11)60117-9
5. W.M. Tucho, V.H. Lysne, H. Austbø, A. Sjolyst-Kverneland, V. Hansen, Investigation of effects of process parameters on microstructure and hardness of SLM manufactured SS316L, J. Alloys Compd. 740 (2018) 910–925. https://doi.org/10.1016/j.jallcom.2018.01.098.
6. V. Tsakiris, D.V. Edmonds, Martensite and deformation twinning in austenitic steels, Mater. Sci. Eng. A 273–275 (1999) 430–436. https://doi.org/10.1016/S0921-5093(99)00322-6
7. E.I. Galindo-Nava, P.E.J. Rivera-Díaz-del-Castillo, Understanding martensite and twin formation in austenitic steels: A model describing TRIP and TWIP effects, Acta Mater. 128 (2017) 120–134. https://doi.org/10.1016/j.actamat.2017.02.004.
8. J. Gubicza, M. El-Tahawy, Y. Huang, H. Choi, H. Choe, J.L. Lábár, T.G. Langdon, Microstructure, phase composition and hardness evolution in 316L stainless steel processed by high-pressure torsion, Mater. Sci. Eng. A 657 (2016) 215–223. https://doi.org/10.1016/j.msea.2016.01.057.
9. M. Ziętala, T. Durejko, R. Panowicz, M. Konarzewski, Microstructure Evolution of 316L Steel Prepared with the Use of Additive and Conventional Methods and Subjected to Dynamic Loads: A Comparative Study, Materials 13 (2020) 4893. https://doi.org/10.3390/ma13214893.
10. Y.F. Shen, X.X. Li, X. Sun, Y.D. Wang, L. Zuo, Twinning and martensite in a 304 austenitic stainless steel, Mater. Sci. Eng. A 552 (2012) 514–522. https://doi.org/10.1016/j.msea.2012.05.080.
11. X. Guan, S. Qu, H. Wang, G. Cao, A. Feng, D. Chen, Adiabatic Shear Localization in Metallic Materials: Review, Materials 17 (2024) 5365. https://doi.org/10.3390/ma17215365.
12. D. Li, Y. Wei, C. Liu, L. Hou, D. Liu, X. Jin, Effects of High Strain Rate on Properties and Microstructure Evolution of TWIP Steel Subjected to Impact Loading, J. Iron Steel Res. Int. 17 (2010) 67–73. https://doi.org/10.1016/S1006-706X(10)60116-1
13. X. Feng, X. Liu, S. Bai, Y. Tang, Y. Ye, Investigation of dynamic tensile mechanical responses and deformation mechanism at high strain rates in a TWIP steel, J. Mater. Res. Technol. 26 (2023) 639–653. https://doi.org/10.1016/j.jmrt.2023.07.241.
14. W.-S. Lee, C.-Y. Liu, The effects of temperature and strain rate on the dynamic flow behaviour of different steels, Mater. Sci. Eng. A 426 (2006) 101–113. https://doi.org/10.1016/j.msea.2006.03.087.
15. N. Yan, Z. Li, Y. Xu, M.A. Meyers, Shear localization in metallic materials at high strain rates, Prog. Mater. Sci. 119 (2021) 100755. https://doi.org/10.1016/j.pmatsci.2020.100755.
16. M. Liu, Z. Guo, C. Fan, T. Tang, X. Wang, H. Hu, Modeling spontaneous shear bands evolution in thick-walled cylinders subjected to external High-strain-rate loading, Int. J. Solids Struct. 97–98 (2016) 336–354. https://doi.org/10.1016/j.ijsolstr.2016.07.014.

17. Q. Xue, Influence of Explosive-Driven Shock Prestraining on the Microstructural Evolution and Shear Localization of 304 and 316L Stainless Steels, in: AIP Conf. Proc., AIP, Baltimore, Maryland (USA), 2006: pp. 783–786. https://doi.org/10.1063/1.2263439.
18. B. Song, T. Martinez, A.Y. Ku, J. Deitz, P. Noell, Development of Kolsky Tension Bar Based Dynamic Incremental Strain and Singular Strain Loading Capability, Exp. Mech. (2025). https://doi.org/10.1007/s11340-025-01159-0.
19. B. Song, D. Casem, J. Kimberley (eds.), Dynamic Behavior of Materials, Volume 1: Proceedings of the 2013 Annual Conference on Experimental and Applied Mechanics, 1st ed., Springer, Cham, 2014. https://doi.org/10.1007/978-3-319-00771-7